ISSN 2176-5480

22nd International Congress of Mechanical Engineering (COBEM 2013)
November 3-7, 2013, Ribeirão Preto, SP, Brazil
Copyright © 2013 by ABCM

THEORETICAL AND EXPERIMENTAL STUDY OF FLAT HEAT PIPE FOR PEM FUEL CELL COOLING

Marcos Vinício Oro
Edson Bazzo
Laboratory of Combustion and Thermal Systems Enginnering - LabCET
Federal University of Santa Catarina, Florianópolis - SC - Brasil
oro@labcet.ufsc.br, ebazzo@emc.ufsc.br

Abstract. *A thin flat heat pipe capable of transporting heat is analyzed as a reliable alternative for Proton Exchange Membrane Fuel Cell (PEMFC) cooling. The flat heat pipe with an evaporator section and a condenser section includes a sealed casing and deionized water as working fluid. Two microgrooves provide the required capillary pumping of the working fluid. In this work a numerical and experimental analysis are presented. A heat transfer model is proposed using existing software to evaluate the capillary limit, the temperature operation and the required working fluid inventory. The main goal is to cool the PEM fuel cells to ensure a suitable operation in the required temperature range between 70 and 90 ^{o}C. An overheating can lead to the membrane drying, what damages the hydrogen ions transport mechanism and consequently leads to the collapse of the fuel cell. The proposed control system consists of a set of stainless steel flat heat pipes, with 100 mm length, assembled in parallel. Preliminary tests indicated that each heat pipe is able to dissipate up to 10 W, ensuring a suitable operation of the PEMFC between 70 and 90 ^{o}C.*

Keywords: *PEMFC, fuel cell cooling, flat heat pipes, heat transfer analysis.*

1. INTRODUCTION

The technical feasibility of proton exchange membrane fuel cell (PEMFC) still relies on technology solutions that solve the problem associated with their operating limits. PEM fuel cells are strong appeal in use in automobiles, portable devices and even in distributed generation. Among the problems related to the operation, there is a need to control the operating temperature in the range of 70 to 90 ^{o}C in order to avoid damaging the polymeric membrane and to achieve higher efficiency of the cell. Generally the cells are assembled into stacks to increase the power generation, which further complicates the temperature control.

Fuel cells work through an electrochemical process, converting the chemical energy of a substance in electrical and thermal energy. The PEM fuel cell is basically composed of two electrodes (anode and cathode) separated by an electrolyte (polymer membrane). The hydrogen is dissociated on the surface of the anode and the ions H^+ move through the membrane toward the cathode, while the electrons are conducted externally closing the circuit on the cathode side to form together with the oxygen the H_2O product.

The thermal control techniques used are summarized in the air, water or a mixture of water and a coolant forced convection. Due to the low heat transfer capacity, the temperature control systems without phase change in addition to consume higher power fail to maintain uniform operating temperature inside the cell.

In patents applied by Faghri (2005a,b), there are two settings bipolar plates for fuel cells that utilize the heat pipes technology for his thermal control. The first is provided with openings for the insertion of micro heat pipes. The second configuration is a bipartite bipolar plate, provided with longitudinal recesses on its inside and a capillary element for pumping the liquid. In both cases no results were presented to validate the proposed mechanisms.

Vasiliev and Vasiliev-Jr (2008) present various forms of thermal management that can be applied in fuel cells of different sizes and powers. Among the proposed systems are mini and micro heat pipes, loop heat pipe, loop thermosyphon, pulsating heat pipe and sorption heat pipe. The article only introduces the ability of each system without, however, presenting tests to demonstrate their applicability.

Silva *et al.* (2012) proposed a combined system comprising three heat pipes coupled to a capillary pumped loop (CPL) as a substitute for the thermal control of a PEM cells, using acetone and deionized water as working fluid for heat pipes and CPL, respectively. As a result, it was possible to dissipate power of 50 W while maintaining the temperature of the fuel cell module below 90 °C.

Recently, a few papers related to theoretical models have been reported in heat pipes, including micro grooved heat pipes. Suman and Kumar (2005) presented an analytical model developed for fluid flow and heat transfer applied to micro-heat pipes of polygonal shape. As study case, the proposed model was used in two heat pipes of different geometries, triangular and rectangular, showing among other parameters the corresponding liquid velocity, heat flux and capillary limit. Later, Suman (2006) presented a discussion related to startup and shutdown of a V-shaped micro-heat pipe, a detailed analysis of the fill charge and a sensitivity analysis of design parameters and properties of the working fluid on the transient operation. As reported by other authors no experimental results are presented.

ISSN 2176-5480

This paper presents theoretical model and also experimental results related to the use of mini heat pipes as an reliable alternative for the thermal control of PEM fuel cells, with low manufacturing cost and technical feasibility of the industrial viewpoint.

2. THEORETICAL ANALYSIS

This section presents the geometric characteristics of the heat pipe under study, the fundamentals related to capillary limit, as well as simplifying assumptions and boundary conditions necessary for installation of the heat pipes in bipolar plate used in PEMFC.

The theoretical analysis is focused on a thin flat heat pipe proposed as alternative for cooling a PEMFC. The heat pipe has only an evaporator section and a condenser section. The proposed cooling system consists of a set of stainless steel flat heat pipes, with 100 mm length, assembled in parallel. The heat load as well as the number of heat pipes are the goal of this work in order to get a reliable system to absorb the heat generated in PEMFC.

2.1 Geometric parameters

The heat generated into the cell is absorbed by heat pipes located at the interface between the bipolar plates as illustrated in Fig. 1. The bipolar plate is shown in Fig. 1(a), where $2Y$ represents the distance between two heat pipes (HP). The parameter Z is the thickness of the bipolar plate. A grid for finite difference calculations is shown in Fig. 1(b) to find the right number of heat pipes required to keep the temperatures below 90 ºC. Here, C_1 and C_2 represent the height and half-width of the proposed heat pipe, respectively. The physical model of the heat pipe considered in the model is shown in Fig. 1(c), where L_c is the condenser length, L_e is the evaporator length and q" is the heat flux. Also Fig. 1(c) shows the expected meniscus of the working fluid close to capillary limit operation. The total length L_T is shown in Fig. 1(d). The groove geometrical parameters are shown in Fig. 1(e), where α is the groove opening, β is an auxiliary angle used in the simulation, and $r(x)$ is the meniscus radius as function of the heat pipe position. Finally, the hydrodynamic behavior is shown in Fig. 1(f), where τ is the shear stress, P is the pressure, A is the wetted area of the meniscus.

The areas occupied by the liquid and vapor phases, A_L(x) e A_V(x), are given by

$$A_L(x) = r(x)^2 \left[\frac{cos^2(\alpha/2)}{tan(\alpha/2)} - \frac{\pi\beta}{360} + \frac{sin(\beta)}{2} \right] \tag{1}$$

$$A_V(x) = \frac{C_2^2 tan(\alpha)}{2} - A_L(x) \tag{2}$$

The hydraulic diameter d_h is obtained by Eq. (3) where p_k represents the perimeter of each phase, and the subscript k liquid and vapor phases.

$$d_{h;k}(x) = \frac{4A_k(x)}{p_k(x)}, \quad k = L, V \tag{3}$$

$$p_L(x) = r(x) \left(\frac{\beta\pi}{180} + \frac{2}{tan(\alpha/2)} \right) \tag{4}$$

$$p_V(x) = C_2 \left[1 + \frac{1}{cos(\alpha)} \right] + r(x) \left[\frac{\beta\pi}{180} - \frac{2}{tan(\alpha/2)} \right] \tag{5}$$

In the position x = 0, the beginning of the condenser, it is assumed that the meniscus radius assumes its maximum value, r_{max}, being determined by

$$r_{max} = C_2 tan(\alpha/2) \tag{6}$$

2.2 Capillary limit

The maximum heat absorbed by the heat pipes is restricted by the capillary limit, which is reached when the capillary pressure is not able to overcome the pressure drop experienced by the fluid, then the liquid supply to the evaporator becomes insufficient, reaching the pipe dryout.

The hydrodynamic problem associated to this physical model is solved under the following considerations:

ISSN 2176-5480

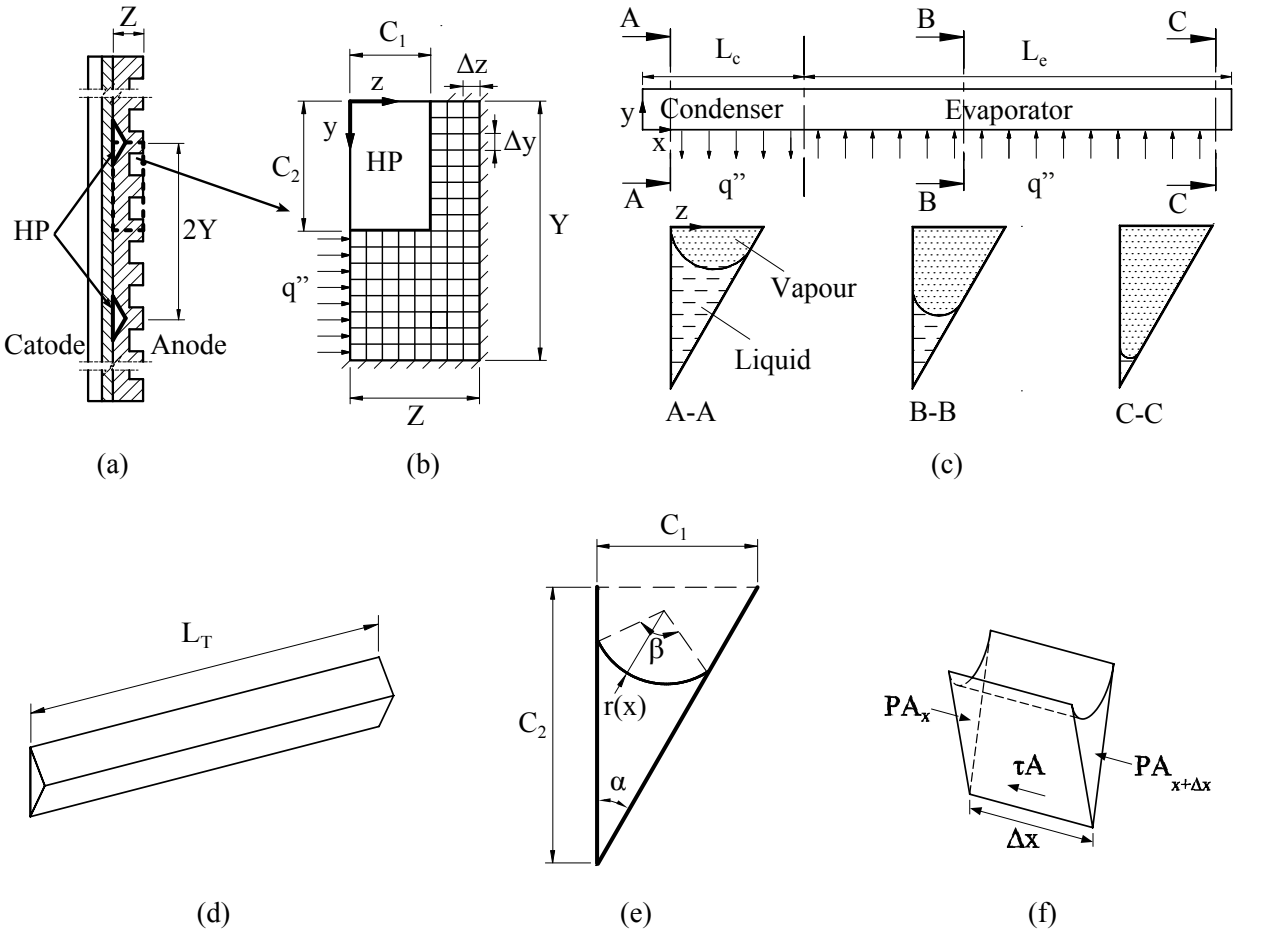

Figure 1. a) Heat pipes arrangement in a bipolar plate; b) Physical model of the bipolar plate; c) Physical model of the heat pipe; d) Proposed geometry of the heat pipe; e) Geometric parameters of a groove; f) Forces acting on the control volume of the liquid.

- One-dimensional model;
- Fully developed laminar flow and incompressible;
- Constant properties;
- Steady state operation;
- Gravitational effects neglected;
- Viscous dissipation neglected;
- Contact angle null;
- Saturated liquid and vapor phases at operating temperature;
- Heat flux uniformly distributed along the condenser and evaporator sections.

Figure 1.(f) shows the forces acting on the control volume of liquid. No interaction is considered at the interface liquid/vapor. Therefore, the balance of force is written as follows:

$$\frac{d(PA)}{dx} = -\tau p \tag{7}$$

where P is the pressure, A is the liquid cross-sectional area, τ is the shear stress of the fluid and p is the wetted perimeter.

From the conservation of mass

$$\dot{m}_L = -\dot{m}_V = \begin{cases} \frac{\dot{q}}{L_c h_{lv}} x & \text{if } 0 \leq x \leq L_c \\ \frac{\dot{q}}{L_e h_{lv}} (L_T - x) & \text{if } L_c < x \leq L_T \end{cases} \tag{8}$$

where $\dot{m}$ is the mass flow rate of the fluid, h_{lv} is the latent heat of vaporization and $\dot{q}$ represents the power applied on the groove, or rejected. Subscripts L and V represent the liquid and vapor phases, respectively.

ISSN 2176-5480

The fluid velocity and shear stress are given by:

$$u = \frac{\dot{m}}{\rho A} \tag{9}$$

$$\tau = \frac{\mu f Re}{2 d_h} \left(\frac{\dot{m}}{\rho A} \right) \tag{10}$$

where ρ and μ represent the density and the dynamic viscosity of the fluid, respectively. Product fRe values were obtained from the model proposed by Etemad and Bakhtiari (1999), which is presented in Appendix.

The solution of Eq. (7) is obtained by dividing the fluid into n control volumes along the axis x. A sufficiently high value of n is used, and it can be assumed that the only variable in the control volume is the pressure. The equation is integrated from x_i to x_{i+1}. The boundary condition used in the first control volume is

$$P_v(x = 0) = P_{sat}(T_{op}) \tag{11}$$

where P_{sat} is the saturation pressure of the fluid at the operating temperature, T_{op}.

The vapor pressure, P_V, and the liquid pressure, P_L, vary along the length of the tube due to the pressure drop experienced by the fluid. The radius of curvature of the meniscus, $r(x)$, is affected by these changes, and, using the Young-Laplace equation, in order to maintain the balance between the phases

$$P_V(x) - P_L(x) = \frac{\sigma}{r(x)} \tag{12}$$

where σ is the surface tension of the fluid.

A general equation is proposed for both phases, liquid and vapor, as well as for both sections, condenser and evaporator, as follows

$$\Delta P_{k;j;i} = P_{k;j;i+1} - P_{k;j;i} = -\frac{2\mu_k f Re_k}{L_j d_{h;k}^2} \left(\frac{\dot{q}}{\rho_k A_k h_{lv}} \right) \psi_{k;j} \qquad k = L, V; \quad j = c, e; \quad i = 1..n \tag{13}$$

where the subscript k represents the liquid (L) or vapor (V) phases, j represents the condenser (c) or evaporator (e) sections, and the ψ parameter is shown in Tab. 1

An iterative method is applied to determine the capillary limit. After certain geometric parameters, using the conditions of Eqs. (6), (8), (11) and (12), the Eq. (13) is solved starting with a low value of power applied that is incremented until $r(x)$ reaches the limit of $r_{min} = 0.02 r_{max}$.

Table 1. $\psi_{k;j}$ parameter used in each control volume i of Eq. (13).

k phase	j section	$\psi_{k;j}$ parameter
L	c	$\frac{x_{i+1}^2 - x_i^2}{2}$
L	e	$L_T \left(x_{i+1} - x_i\right) - \left(\frac{x_{i+1}^2 - x_i^2}{2}\right)$
V	c,e	$-\psi_{L;j}$

The working fluid inventory has an important influence on the performance of the heat pipe. The inventory is determined by

$$m_T = m_L + m_V = V_L \rho_L + V_V \rho_V \tag{14}$$

where V is the volume of each phase, given by

$$V_k = \sum_{i=1}^{n} V_{k;i} = \sum_{i=1}^{n} A_{k;i} \Delta x \qquad k = L, V \tag{15}$$

ISSN 2176-5480

In order to know the optimum amount of fluid that should be inserted in the pipe, in this work will be evaluated the filling ratio, FR, which is determinated by

$$FR = \frac{V_{L;in}}{V_T} \tag{16}$$

where $V_{L;in}$ is the liquid volume which is inserted in heat pipe at room temperature and V_T is the heat pipe inner total volume.

Note that the Eq. (15) provides the volumes at operation temperature, but on filling procedure it is necessary to know the required volume at room temperature. Then, the values given by Eq. (15) are updated for the room temperature. The sum of these new values gives the $V_{L;in}$.

2.3 Temperature distribution in the bipolar plate

The physical model to determine the distribution of heat pipes along the interface of the bipolar plate is proposed as shown in Fig. 1.(b), where the hatched area represents the bipolar plate, C_1 the heat pipe height, C_2 the heat pipe half-width and q" the heat flux generated in the cell. The white region comprises half of the heat pipe cross section (HP). To simplify the model, the geometry of the heat pipe was considered rectangular, and the gases channels are treated as a solid with properties equal to those of the bipolar plate. The heat transfer problem associated with the physical model is solved under the following assumptions:

- Steady-state conditions;
- Two-dimensional conduction;
- Constant properties;
- Internal heat generation null;
- Heat pipe temperature equal to the heat pipe wall temperature (T_w);
- Heat pipe with rectangular profile;
- Bipolar plate gas flow channels with equal properties to those of the bipolar plate.

The governing equation to solve the problem is

$$\frac{\partial^2 T}{\partial y^2} + \frac{\partial^2 T}{\partial z^2} = 0 \tag{17}$$

subjected to the following boundary conditions:

$$T = T_w \quad \text{for} \quad 0 \leq y \leq C_2 \ \text{ and } \ 0 \leq z \leq C_1 \tag{18}$$

$$\frac{\partial T}{\partial y} = 0 \quad \text{for} \quad y = 0 \ \text{ and } \ C_1 < z \leq Z \tag{19}$$

$$\frac{\partial T}{\partial y} = 0 \quad \text{for} \quad y = Y \ \text{ and } \ 0 \leq z \leq Z \tag{20}$$

$$-k\frac{\partial T}{\partial z} = \dot{q}'' \quad \text{for} \quad z = 0 \ \text{ and } \ C_2 \leq y \leq Y \tag{21}$$

$$\frac{\partial T}{\partial z} = 0 \quad \text{for} \quad z = Z \ \text{ and } \ 0 \leq y \leq Y \tag{22}$$

The temperature distribution at the interface of the fuel cell was calculated by finite difference method, considering a two-dimensional steady state heat conduction. The mesh was refined in order to ensure a temperature tolerance less than 0.05 ^{o}C. The problem is solved by varying the Y value to obtain a preset temperature difference between points of higher and lower temperature, $\Delta T_{max} = T(Y, 0) - T(0, 0)$.

ISSN 2176-5480

3. SETUP EXPERIMENTAL

The cooling system of the cell comprises a set of heat pipes assembled in parallel. The heat pipes are made from stainless steel tubes (316L) with 3.175 mm outside diameter and 0.25 mm wall thickness. The total length is 100 mm. The condenser and evaporator lengths are 30 and 70 mm, respectively. The pipes are shaped in a special matrix, giving the format shown in Fig. 1(d), where two micro-grooves are formed with the ability to provide the required capillary pumping. The working fluid is deionized water. The heat pipes underwent a standard ultrasonic cleaning process using an Odontobras^{TM} 2840D ultrasonic cleaner. Then, the pipes are evacuated using an Edwards^{TM} E2M18 pump and loaded with deionized water. Thermocouples Omega^{TM} T-type are mounted along the tubes.

A computer connected to an Agilent^{TM} 34970A acquisition system was used for the temperature acquisition. The system power supply was an Agilent^{TM} N6700B and the resistance was a constantan wire. The condenser was assembled using a standard Microbon^{TM} 12 VDC coolers designed for a CPU microprocessor. The evaporator section was insulated with a fiberglass layer and an expanded polymer layer (Polipex^{TM}).

An existing 200 W Electrocell^{TM} fuel cell in operation at LabCET was taken as reference in this work. Ten units 20 W fuel cells are combined to form the fuel cell stack. The efficiency was considered 50%. So 20 W is the thermal power to be absorbed by the heat pipes in each unit cell.

Different heat pipes were tested in order to know his behaviour and heat load capacity at working temperatures below 90 ^{o}C. In this paper the corresponding results are presented for two heat pipes. Conduction tests were previously performed without working fluid, whereby the tube it self is able to dissipate by axial conduction about 2 W. Both were loaded with a 20% filling ratio. The thermocouples positioning is shown in Fig. 2. The tests were performed by applying power in steps. In the HP1 case, power input of 2, 3, 4, 5, 6 and 7 W were used. Int the HP2 case, the power input were 2, 4, 6, 8 and 10 W.

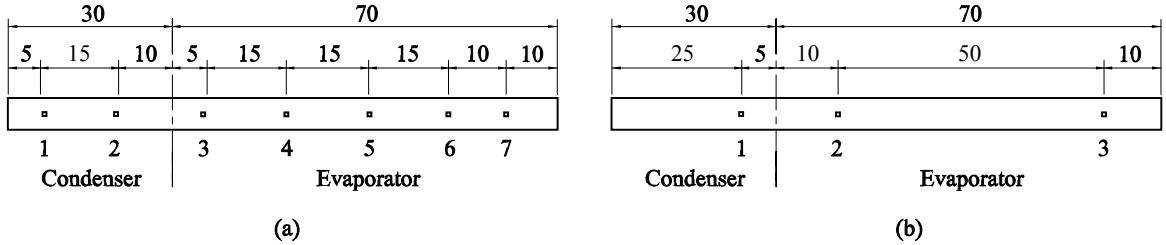

Figure 2. Thermocouples positioning. a) HP1; b) HP2 (units in mm).

The expanded measurement uncertainties were estimated with 95% confidence interval. The power input uncertainty associated was estimated as $\pm$ 0.2 W. The temperature uncertainty was evaluated taking into account the uncertainty of the thermocouples, acquisition system and the statistical uncertainty related to the number of experiments. In the HP1 case, the maximum uncertainty was $\pm$ 6.0 ^{o}C on thermocouple 6. In the HP2 case, the maximum was $\pm$ 3.9 ^{o}C on thermocouple 2.

4. RESULTS AND DISCUSSION

Two simplified models has been presented. A fluid hydrodynamic analysis to estimate the capillary limit and a two-dimensional heat transfer model to determine the required number and spacing between the heat pipes. Tests were performed to evaluate the heat pipe thermal behavior.

Power is applied onto the evaporator section, where the working fluid evaporates and goes to the condenser section. The corresponding pressure drops of both phase are considered in this work. The higher the heat load, the higher the pressure drops. In the same way the higher the pressure drop the lower the meniscus radius, as considered in the model. The conditions used to analyse the capillary limit were: n = 100; T_{op} = 80 °C; α = 30 °; L_c = 30 mm; L_e = 70 mm; C_1 = 1.126 mm; C_2 = 1.950 mm. It was considered that the capillary limit is reached when $R_{min} = 0.02 R_{max}$, providing R_{min} = 0.01 mm. The dimensions C_1 and C_2 are related with the inner perimeter of a circular tube, which has an outside diameter of 3.175 mm and 0.25 mm thickness.

Applying the proposed model under these conditions the heat pipe is able to dissipate up to 12.5 W, and the optimal required filling ratio is 18.0%. The pressure distribuition of the liquid and vapor phases along the heat pipe are presented in Fig. 3. As noted, the highest pressure drop ocurr along the microgrooves in the liquid phase. That is because the meniscus recede, causing a fast decreasing of the wetted area and so the fast increasing of the liquid velocity, as shown in Fig. 4.

Figure 5 shows the fRe behavior for both phases. In the liquid case it remains constant, while for the vapor it has a particular behavior. The reasons are because in the liquid all the geometric parameters vary proportionally, and in the vapor, because the d_{insc} is constant while the geometric parameter vary. Figure 6 presents the meniscus radius behavior

ISSN 2176-5480

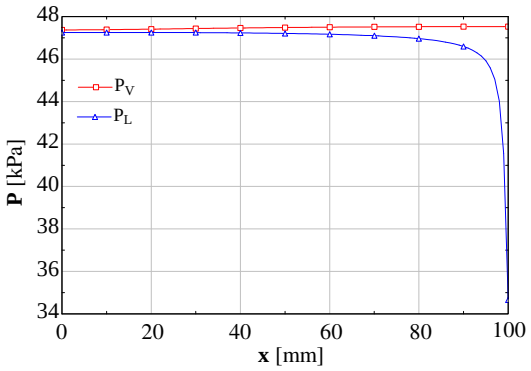

Figure 3. Pressures behavior along the HP.

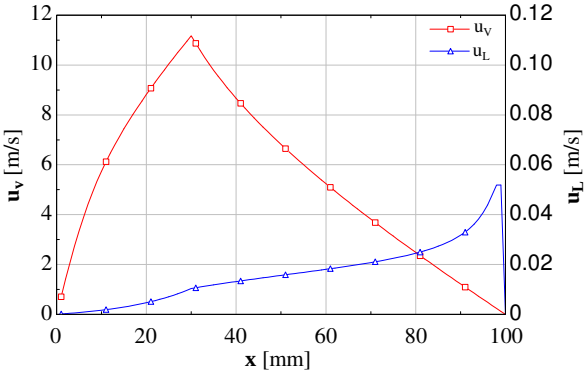

Figure 4. Velocities profiles along the HP.

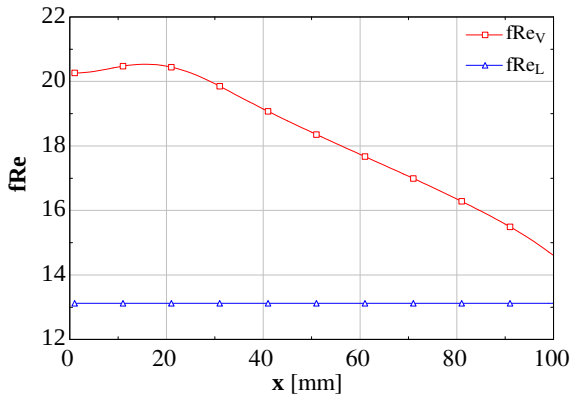

Figure 5. fRe_k behavior along the HP.

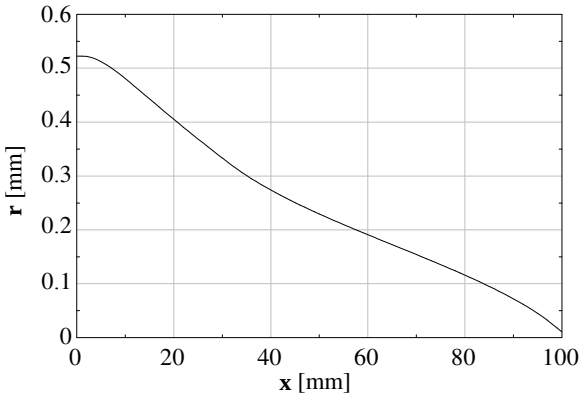

Figure 6. Radius of curvature behavior along the HP.

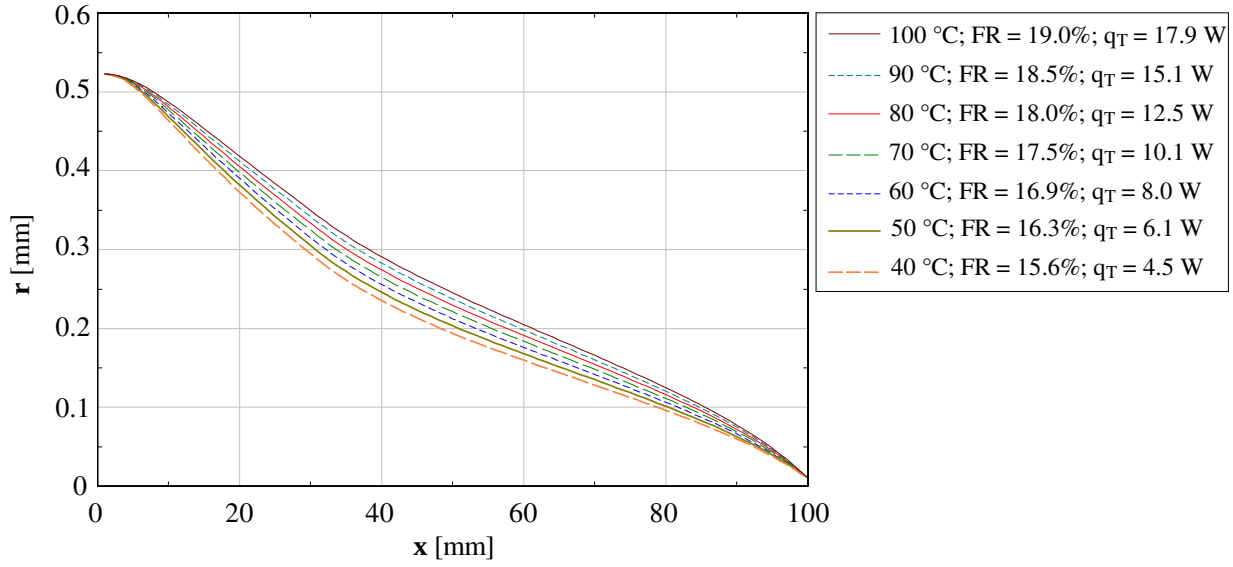

Figure 7. Meniscus radius behavior along the HP with differents operation temperature values.

along the heat pipe when the cappilary limit condition is reached at 80 °C. The capillary limit was also evaluated in the range of 40 to 100 °C, keeping constant the other parameters. The correct charging of the heat pipe has been also object of concern. As observed in Fig. 7 the capillary limit is strongly dependent of the filling ratio. Figure 7 shows the meniscus radius behavior along the heat pipe for each temperature. At lower temperature, the heat pipe can dissipate 4.5 W, requiring 15.6% of filling ratio (FR) and meniscus radius has the lowest values along the tube. As temperature increases, the power dissipation increases, but this requires larger amount of the working fluid. Therefore the values of the meniscus radius along the HP is greater at higher temperatures. A comparison between the variation of the power dissipated and the FR with the desired operating temperature is shown in Fig. 8. Note that the increase in power is much higher than in FR. As the temperature increases 150%, the FR and the power increase 21 and 295%, respectively. These

ISSN 2176-5480

behavior are related with the liquid transport factor, LTF (also called figure of merit or merit number), which is increasing in the evaluated temperature range. Thus, for the conditions evaluated, the cappilary limit increases as the FR.

As stated before, the influence of the working fluid inventory on the capillary limit and the operation temperature was also evaluated. Figure 9 shows the meniscus radius behavior along the heat pipe from condenser section to evaporator section, considering the filling ratio of 18, 20, 22 and 24%, for operation temperature set at 60, 70 and 80 °C. The highest measured power input (12.5 W) was achieved for FR = 18%, which corresponds to the capillary limit condition. For every filling ratio, it is interesting to note the inversion behavior of the curves close to 60 mm. The reason for that is still under investigation and it was not the focus of this paper. According to the experimental results, in the tested range any choice of filling ratio is reliable for the pupose of this work, and 20% was the chosen filling ratio.

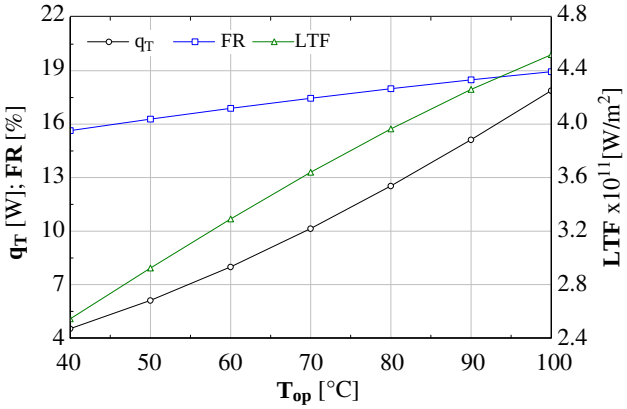

Figure 8. Relation between power dissipated, filling ratio and liquid transport factor at different temperatures in cappilary limit condition.

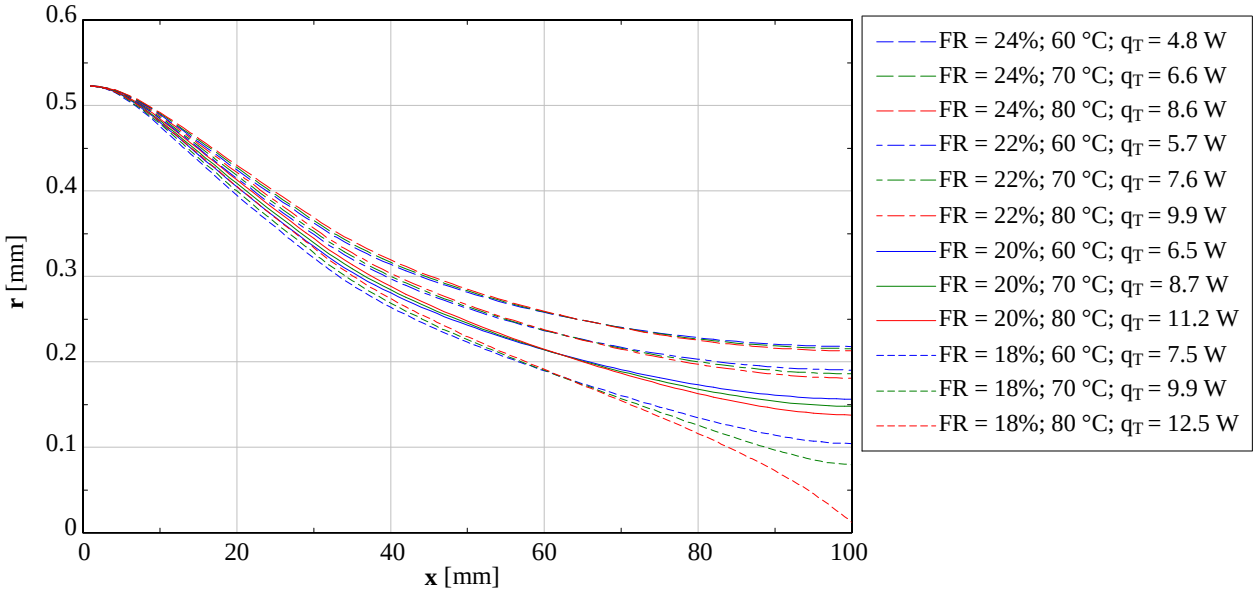

Figure 9. Operation temperature sensivity for different working fluid inventory.

Different heat pipes were performed in the laboratory, considering the PEMFC operation temperature as the limit for stop the power input increasing. The experimental results conserning two heat pipes are presented in Figs. 10 and 11. The first heat pipe, HP1, reached 7 W. The evaporator section presented an atypical behavior, because of accentuated variation in temperature. Some problem in isolation may have caused this changes. The second heat pipe, HP2, was able to dissipate 10 W. In this case, the HP had a normal behavior, with a small increase in temperature along the evaporator section. The difference between HP2 and HP1 power may have come from the filling process given the small quantity to be loaded ($<$100 μl).

In the Figs. 10 and 11 were added dashed lines, which correspond to the temperature value obtained from the theoretical model for the respective powers, being 62.2 °C for 7 W and 75.2 °C for 10 W. The figures show that the model represents the experimental behavior, especially in the second case. It should be taken into account that the theoretical model refers only to the temperature of the working fluid, which is considered constant throughout the length of the pipe,

ISSN 2176-5480

while the experimental data refer to the heat pipe wall temperature.

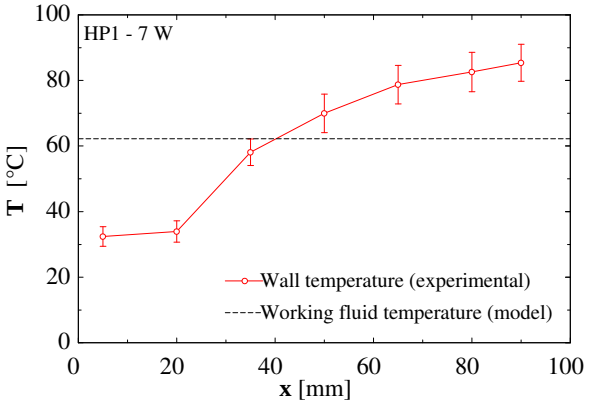

Figure 10. Temperature distribution along the HP1.

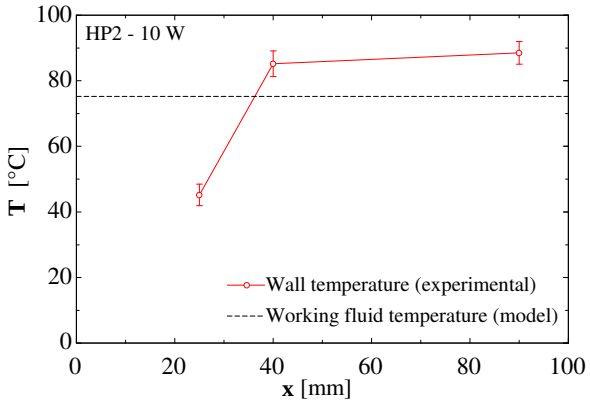

Figure 11. Temperature distribution along the HP2.

Comparing the experimental data with the theoretical, it is observed that the temperature difference in the condenser section is greater than in the evaporator section. From the average temperature in each section of HP1, there is an difference with the model of 47% in condenser section and 20% in evaporator section. For HP2, the differences are 40 and 15% for the respective sections. A better comparison would be possible with the improvement of the model to evaluate the thermal resistance between the fluid and the outer wall of the pipe. The corresponding thermal resistences were calculated equal to 6.0 and 4.2 °C/W for HP1 and HP2, respectively.

The second theoretical model was used to determine the heat pipe required amount and the distance between them at the interface of a bipolar plate. The conditions used were: heat pipe temperature equal to 80 °C; the unit cell generating 20 W in 100 cm^2 area resulting q" = 2000 W/m^2; $C_1 = C_2 = 2$ mm; $Z = 4$ mm; the bipolar plate thermal conductivity equal to 100 W/m/K; $\Delta y = \Delta z = 0.2$ mm and $\Delta T_{max} = 5$ °C. The solution provides that each heat pipe will absorb 12.6 W with a distance $2Y = 90$ mm. Taking into account the area of 100 cm^2 and considering the cell with equal length of the heat pipe evaporator section, $L_e = 70$ mm, the cell resultant height is 143 mm. Thus, two heat pipes are required in the bipolar plate interface and a new distance is calculated, obtaining $2Y = 72$ mm with $\Delta T_{max} = 3.1$ °C and $q_T = 10$ W. Finally, comparing with the experimental data, three heat pipes are required to remove the heat from the unit fuel cell. Whereby the results are: $2Y = 48$ mm, $\Delta T_{max} = 1.3$ °C and $q_T = 6.7$ W, providing uniformity in the operating temperature of the PEMFC and showing the applicability of the proposed cooling system.

5. CONCLUSIONS

A thin flat heat pipe was analyzed as a reliable alternative for proton exchange membrane fuel cell cooling. The theoretical results are in good agreement with experimental results. Power up to 10 W were measured using deionized water as the working fluid. The tests with the proposed heat pipes were considered successful, attending the required heat dissipation and the optimum temperature operation for the PEMFC, although further tests are required. As expected, the operating temperatures were calculated at intermediate values between the measured temperatures in the evaporator and condenser. Looking at the experimental results, it were found differences in the range of 40-47% at the condenser and 15-20% at the evaporator, relatively to the working fluid temperature calculated. It has been shown that the theoretical models have been useful in the design of the PEMFC cooling system.

6. APPENDIX

The model used for the determination of product fRe for each phase was proposed by Etemad and Bakhtiari (1999). First define the dimensionless parameters:

$$d_* = \frac{d_h}{d_{ins}} \tag{A1}$$

$$N_* = \frac{A_k}{A_d} \tag{A2}$$

where d_h, d_{ins}, A_k e A_d represent the hydraulic diameter, the largest diameter inscribed within the fluid channel, the area occupied by the fluid and the area based on the hydraulic diameter, respectively. The product fRe is determined by making use of a few constants as follows

ISSN 2176-5480

$$fRe = a_0 + a_1 d_* + a_2 {d_*}^2 + a_3 {d_*}^3 + a_4 {d_*}^4 + a_5 {d_*}^5 + a_6 N_* + a_7 {N_*}^2 + a_8 {N_*}^3 + a_9 {N_*}^4 + a_{10} {N_*}^5 \quad \text{(A3)}$$

where a_0 = -28,48854; a_1 = 268,72899; a_2 = -476,29475; a_3 = 396,33079; a_4 = -155,13995; a_5 = 23,37618; a_6 = -21,00613; a_7 = 10,62318; a_8 = -2,51512; a_9 = 0,27889 e a_10 = -0,01167.

This model was chosen because it has good agreement with literature data for various geometric shapes, obtaining relative errors lower than 10%.

7. ACKNOWLEDGEMENTS

Thanks to Coordination for the Improvement of Higher Level Personnel (CAPES) for financial support.

8. REFERENCES

Etemad, S.G. and Bakhtiari, F., 1999. "General equations for fully developed fluid flow and heat transfer characteristics in complex geometries". *International Communications in Heat and Mass Transfer*, Vol. 26, No. 2, pp. 229–238.

Faghri, A., 2005a. "Micro heat pipe embedded bipolar plate for fuel cell stacks". US Patent Application 20050026015, Feb. 03 2005.

Faghri, A., 2005b. "Integrated bipolar plate heat pipe for fuel cell stacks". US Patent Application 20050037253, Feb. 17 2005.

Silva, A.P., Galante, R.M., Pelizza, P.R. and Bazzo, E., 2012. "A combined capillary cooling system for fuel cells". *Applied Thermal Engineering*, Vol. 41, pp. 104 – 110. 13th Brazilian Congress of Thermal Sciences and Engineering.

Suman, B., 2006. "On the fill charge and the sensitivity analysis of a v-shaped micro heat pipe". *AIChE Journal*, Vol. 52, No. 9, pp. 3041–3054.

Suman, B. and Kumar, P., 2005. "An analytical model for fluid flow and heat transfer in a micro-heat pipe of polygonal shape". *International Journal of Heat and Mass Transfer*, Vol. 48, No. 21–22, pp. 4498 – 4509.

Vasiliev, L. and Vasiliev-Jr, L., 2008. "Heat pipes in fuel cell technology". In S. Kakaç, A. Pramuanjaroenkij and L. Vasiliev, eds., *Mini-Micro Fuel Cells*, Springer Netherlands, NATO Science for Peace and Security Series C: Environmental Security, pp. 117–124.

9. RESPONSIBILITY NOTICE

The authors are the only responsible for the printed material included in this paper.